34 *Journal of Electrical Engineering & Technology Vol. 7, No. 1, pp. 34~45, 2012*
http://dx.doi.org/10.5370/JEET.2012.7.1.34

Speed Control of Linear Induction Motor using Sliding Mode Controller Considering the End Effects

A. Boucheta†, I. K. Bousserhane*, A. Hazzab*, P. Sicard and M. K. Fellah*****

Abstract – In the present paper, the mover speed control of a linear induction motor (LIM) using a sliding mode control design is proposed, considering the end effects. First, the indirect field-oriented control LIM is derived, considering the end effects. The sliding mode control design is then investigated to achieve speed- and flux-tracking under load thrust force disturbance. The numerical simulation results of the proposed scheme present good performances in comparison to that of the classical sliding mode control.

Keywords: Linear induction motor, End effects, Compensation, Field-oriented control, Sliding mode control

1. Introduction

Currently, linear induction motors (LIMs) are widely used in many industrial applications, including transportation, conveyor systems, actuators, material handling, pumping of liquid metal, sliding-door closers, and others, with satisfactory performance [1, 2]. The most obvious advantage of a linear motor is that it has no gears and requires no mechanical rotary-to-linear converters. Linear electric motors can be classified into the following: DC motors, induction motors (IM), synchronous motors, stepping motors, and others. An LIM has many advantages, such as high-starting thrust force, alleviation of gear between motor and the motion devices, reduction of mechanical losses and the size of motion devices, high-speed operation, silence, and so on [1-4]. The driving principles of an LIM are similar to those of a traditional rotary induction motor (RIM); however, its control characteristics are more complicated. The motor parameters are time-dependent because of changes in the operating conditions, such as the speed of the mover, temperature, and rail configuration. Moreover, significant parameter variations exists in the reaction rail resistivity, the dynamics of the air gap, slip frequency, phase unbalance, saturation of the magnetizing inductance, and end effects [1-3, 5]. Therefore, its mathematical model is difficult to derive completely.

An equivalent circuit modeling of an LIM is not simple as that of a rotary motor because of the existence of the end effect. In RIMs, a sufficiently accurate equivalent circuit model can be made because of the pole-by-pole symmetry. However, in LIMs, the pole symmetry argument is not preserved because the electrical conditions change at the entry and exit point because of the end effect [6-8]. A significant amount of research has been conducted for the modeling of the dynamic performance of the LIM and all significant variations have been taken into consideration [1, 2, 4, 5]. However, uncertainties continue to exits, which are usually composed of unpredictable plant parameter variations, external load disturbance, unmodeled and nonlinear dynamics, in practical applications of the LIM. Most of the existing models of an LIM depend on field theory [6-10]; hence, they cannot be directly applied for vector control. Many researchers have derived "per-phase" equivalent circuits reflecting the end effect [6-8]. The field theory was utilized in developing the lumped parameter of the LIM model [7-9], wherein end effect, field diffusion in the secondary sheet, skin effect, and back-iron saturation were considered. However, the resulting lumped-parameter models were very complicated for practical use in modeling and control.

To resolve the unique end-effect problem, speed-dependent scaling factors are introduced to the magnetizing inductance and series resistance in the d-axis equivalent circuit of the RIM to correct the deviation caused by the end effect [11]. In contrast, a thrust correction coefficient introduced by [12] can be used to calculate an actual thrust to compensate for the end effect. A related method to deal with the problem is the introduction of an external force corresponding to the end effect into the RIM model to provide a more accurate modeling of an LIM considering the end effect, as shown in [13]. In another work [14], the authors proposed a new type of end-effect compensator. The proposed method is based on the new concept that the end effect can be compensated only by supplying the eddy

† Corresponding Author: Laboratory of Command, Analysis and Optimization of Electro-Energetic Systems, University of Bechar B.P 417 Bechar 08000, Algeria. (boucheta_ak@yahoo.fr)
* Laboratory of Command, Analysis and Optimization of Electro-Energetic Systems, University of Bechar B.P 417 Bechar 08000, Algeria.
** Groupe de recherche en électronique industrielle, École d'Ingénierie, Département de Génie électrique et Génie informatique. Université du Québec á Trois-Rivières, Canada. (pierre.sicard@uqtr.ca)
*** University of Djillali Liabes, BP 98 Sidi Bel-Abbes, Algeria.
Received: September 10, 2010; Accepted: July 29, 2011

current synchronizing with the LIM frequency in front of the LIM.

The field-oriented control (FOC) technique has been widely used in the industry for high-performance IM drives [7, 8]. The technique can provide the same performance as that of separately excited DC machines [9-11]. The knowledge of synchronous angular velocity is often necessary in phase transformation to achieve the favorable decoupling control between motor torque and rotor flux for a separately excited DC machine. This technique can be performed using two basic methods: direct vector control and indirect vector control. Both direct field-oriented (DFO) and indirect field-oriented (IFO) solutions have been implemented in industrial drives demonstrating performances suitable for a wide spectrum of technological applications [8, 15-17]. However, the performance of these solutions is sensitive to the variation of motor parameters, especially the rotor time constant, which varies with the temperature and the saturation of the magnetizing inductance. Recently, much attention has been given to the possibility of identifying the changes in motor parameters of LIM while the drive is in normal operation. This stimulated significant research activities to develop LIM vector control algorithms using nonlinear control theory to improve performances, to achieve speed (or torque) and flux tracking, or to provide a theoretical justification for the existing solutions [1,15,18,19].

Sliding mode control (SMC) is one of the prospective control methodologies for electrical machines because of its order reduction, disturbance rejection, and strong robustness, along with its simple implementation through power converters [20-22]. SMC is a type of variable structure scheme that involves switching between controllers. In general, the design of variable structure controllers consists of two steps: the reaching and sliding phases [20]. First, the system is directed towards a switching surface by a feedback-control law. A switching term is then used to maintain sliding mode, during which the dynamics of the system are determined by the choice of sliding surface. The sliding mode is relatively independent of parametric uncertainties and load disturbances. SMC has been employed for position and speed control of AC machines. However, the discontinuous nature of the switching feature of SMC causes chattering in the control system [20, 21].

In the present paper, a sliding mode controller based on indirect field orientation is proposed for LIM speed control while considering end effects. The proposed controller is applied to achieve a speed- and flux-tracking objective under parameter uncertainties and disturbance of load thrust force. The reminder of the current paper is organized as follows: Section 2 reviews the principle of the indirect field-oriented control (IFOC) of LIM considering the end effects. Section 3 highlights the development of sliding mode controllers design for LIM speed control. Section 4 discusses simulation results. Conclusions are drawn in Section 5.

2. Indirect Field-oriented Control of the LIM

The primary (mover) of the adopted three-phase LIM is simply a "cut-open-and-rolled-flat" rotary-motor primary. The secondary generally consists of a sheet conductor using aluminium with an iron back for the return path of the magnetic flux. The primary and secondary form a single-sided LIM. Moreover, a simple linear encoder is adopted for the feedback of the mover position.

Fig. 1(a) shows a conceptual construction of an LIM. In an LIM, as the primary moves, the secondary is continuously replaced by a new material that tends to resist a sudden increase in flux penetration and only allows a gradual build up of the flux density in the air gap. To obtain a suitable LIM equivalent circuit, quantifying the effects of the entry and exit of new material on the air gap flux distribution known as the end effect will be necessary. When the primary of an LIM does not move, there is no difference in the equivalent circuits of LIM and RIM, because the contribution of the end effects will be relatively small and can be neglected. However, if the primary coil of LIM moves, a new field penetrates into the reaction rail in the entry area, whereas the existing field disappears at the exit area, thereby creating the eddy current in the reaction rail. The eddy current in the entry grows very rapidly to mirror the primary current, nullifying

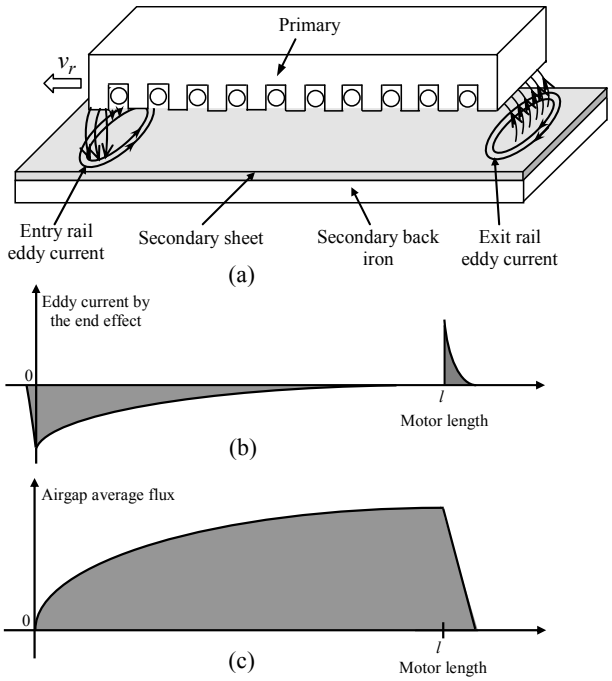

Fig. 1. (a) Eddy current at the entry and exit of the air gap for a given velocity; (b) Polarity and decaying profile of the entry and exit eddy currents; (c) Air gap flux profile

the primary magneto motive force (MMF) and reducing the flux to nearly zero at entry [6-8]. At the same time, the eddy current generates dragging force at the exit area, which reduces the hauling ability of the motor. The density profile of the eddy current along the length of LIM is depicted in Fig. 1(b) [6-8]. Hence, the resulting MMF, and thereby air gap flux, is something similar to that shown in Fig. 1(c).

The spatial distribution of the magnetic flux density along the length of the primary is dependent on the relative velocity between the primary and the linor (secondary). For a zero relative velocity, the LlM can be considered to have an infinite primary. In this case, the end effects may be ignored. The end-effect dynamic because of the relative motion between the primary and the secondary causes additional thrust attenuation, which may decrease the main thrust force of the LIM. At low speed, the additional thrust attenuation are small; at high speed, the additional thrust attenuation becomes significant [6-10].

The end effects behave differently at the entry and exit ends of the LIM. The currents induced in the secondary at the entry end decay more slowly than at the exit end because of a larger time constant. Duncan used the parameter Q to simulate this effect associated with the length of the primary. To a certain degree, he quantified the end effects as a function of the velocity v_r as described by Eq. (1) [7-10]:

$$Q = \frac{l \cdot R_r}{L_r \cdot v_r} \tag{1}$$

where l is the primary length.

Note that the motor length is clearly dependent on the motor velocity. As the velocity increases, the primary's length decreases, increasing the end effects, which reduces the LIM's magnetization current. The magnetizing inductance can then be deduced, as shown below [6, 8]:

$$L_m^{'} = L_m(Q) = L_m\left(1 - f(Q)\right) \tag{2}$$

where L_m is the magnetizing inductance at zero speed and $f(Q) = \left(1 - e^{-Q}\right)/Q$.

The secondary and primary inductances are expressed as [7, 8]

$$L_r^{'} = L_r(Q) = L_r - L_m f(Q) \tag{3}$$

$$L_s^{'} = L_s(Q) = L_s - L_m f(Q) \tag{4}$$

The secondary time constant is given by

$$\tau_r^{'} = L_r^{'}/R_r = L_r/R_r - L_m \cdot f(Q)/R_r \tag{5}$$

The dynamic model of the LIM developed by Duncan is analyzed using the d-q model of the equivalent electrical circuit including the end effects [7, 9, 10, 23]. The q-axis equivalent circuit of the LIM is identical to the q-axis equivalent circuit of the RIM. In this case, the parameters do not vary with the end effects. However, the d-axis entry linoric currents affect the air gap flux by decreasing ϕ_{dr}. Therefore, the d-axis equivalent circuit of the RIM cannot be used in the LIM analysis when the end effects are considered.

Fig. 2(a) shows the d-axis equivalent, wherein the magnetization branch differs from that of the traditional induction motor. In Fig. 2(b), the equivalent circuit is the same as that in the traditional induction motor. From the d-q equivalent circuit of the LIM (Fig. 2), the primary and secondary voltage equations in a synchronous reference system aligned with the secondary flux are given by [7, 9, 10, 23]

$$v_{ds} = R_s i_{ds} + R_r f(Q)\cdot\left(i_{ds} + i_{dr}\right) + p\phi_{ds} - \omega_e \phi_{qs} \tag{6}$$

$$v_{qs} = R_s i_{ds} + p\phi_{qs} + \omega_e \phi_{ds} \tag{7}$$

$$v_{dr} = R_r i_{dr} + R_r f(Q)\cdot\left(i_{ds} + i_{dr}\right) + p\phi_{dr} - \left(\omega_e - \omega_r\right)\phi_{qr} = 0 \tag{8}$$

$$v_{qr} = R_r i_{qr} + p\phi_{qr} + \left(\omega_e - \omega_r\right)\phi_{dr} = 0 \tag{9}$$

The linkage fluxes are given by the following equations:

$$\phi_{ds} = L_{ls} i_{ds} + L_m\left(1 - f(Q)\right)\left(i_{ds} + i_{dr}\right) \tag{10}$$

$$\phi_{qs} = L_{ls} i_{qs} + L_m\left(i_{qs} + i_{qr}\right) \tag{11}$$

$$\phi_{dr} = L_{lr} i_{dr} + L_m\left(1 - f(Q)\right)\left(i_{ds} + i_{dr}\right) \tag{12}$$

$$\phi_{qr} = L_{lr} i_{qr} + L_m\left(i_{ds} + i_{dr}\right) \tag{13}$$

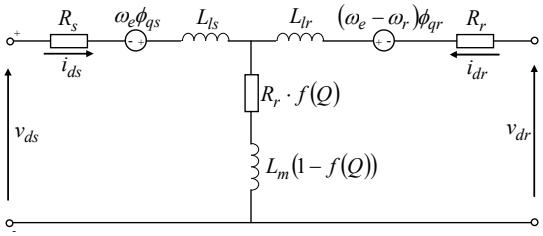

(a) d-axis equivalent circuit

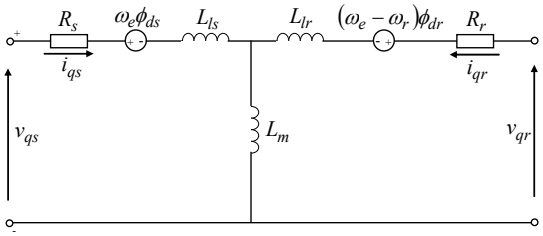

(b) q-axis equivalent circuit

Fig. 2. LIM equivalent circuits taking into account the end effects.

The thrust force is expressed as

$$F_e = \frac{3}{2} P \frac{\pi}{h} \frac{L_m \left(1 - f\left(Q\right)\right)}{L_r - L_m f\left(Q\right)} \left(\phi_{dr} i_{qs} - \phi_{qr} i_{ds}\right) = M \cdot \dot{v}_r + D \cdot v_r + F_L \tag{14}$$

As in DC machines, the main objective of the vector control of LIMs is to independently control the thrust force and the flux; this is accomplished using a *d-q* rotating reference frame synchronously with the primary flux space vector [8, 15, 16, 17]. In ideal FOC, the secondary flux linkage axis is forced to align with the d-axis. Thus,

$$\phi_{qr} = \frac{d\phi_{qr}}{dt} = 0 \tag{15}$$

$$\phi_{dr} = \phi_r = \text{constant} \tag{16}$$

where ϕ_r is the nominal primary flux.

With the use of the IFOC technique and considering that the electrical time constant is much smaller than the mechanical time constant, the thrust force shown in (14) can be reasonably represented by the following equations:

$$F_e = K_f \cdot i_{qs} \tag{17}$$

$$K_f = \frac{3}{2} P \frac{\pi \cdot L_m \left(1 - f\left(Q\right)\right)}{h \cdot \left(L_r - L_m f\left(Q\right)\right)} \phi_{dr} \tag{18}$$

where K_f is the force constant.

Moreover, using (8), the feed-forward slip velocity signal can be estimated using ϕ_{dr} and i_{qs} as follows:

$$v_{sl} = \frac{h \cdot L_m \left(1 - f\left(Q\right)\right)}{\pi \cdot \left(L_r / R_r - L_m f\left(Q\right) / R_r\right)} \frac{i_{qs}^*}{\phi_{dr}} \tag{20}$$

where the superscript '*' represents the reference values.

The decoupling control method with compensation chooses the inverter output voltages such that

$$v_{ds}^* = \left(K_p + K_i \frac{1}{s}\right)\left(i_{ds}^* - i_{ds}\right) - \frac{\pi}{h} v_e L_\sigma \left(Q\right) i_{qs}^* \tag{21}$$

$$v_{qs}^* = \left(K_p + K_i \frac{1}{s}\right)\left(i_{qs}^* - i_{qs}\right) + \frac{\pi}{h} v_e L_\sigma \left(Q\right) i_{ds}^* + \frac{P \cdot L_m}{L_r} \frac{\pi}{h} v_r \phi_{dr} \tag{22}$$

where $L_\sigma\left(Q\right)$ is the total leakage inductance denoted by

$$L_\sigma\left(Q\right) = L_s - L_m f\left(Q\right) - \frac{\left(L_m \left(1 - f\left(Q\right)\right)\right)^2}{L_r - L_m f\left(Q\right)} \tag{23}$$

According to the above analysis, the IFOC of LIM considering end effects can reasonably be presented by the block diagram shown in Fig. 3.

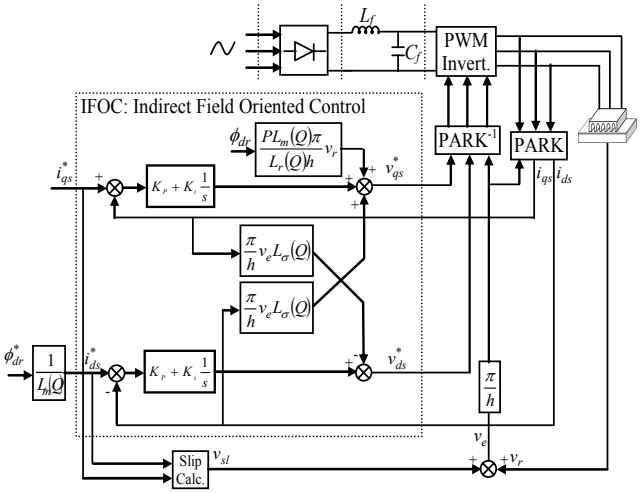

Fig. 3. Block diagram of IFOC for LIM

3. Speed Control of LIM using Sliding Mode Control

3.1 Sliding mode control

Variable structure control (VSC) with sliding mode (SMC) is one of the effective nonlinear robust control approaches because it provides system dynamics with an invariance property to uncertainties once the system dynamics are controlled in the sliding mode [20-25]. The first step of SMC design is to select a sliding surface that models the desired closed-loop performance in state-variable space. The control is then designed such that the system state trajectories are forced to the sliding surface and to stay on it. The system state trajectory in the period of time before reaching the sliding surface is called the reaching phase. Once the system trajectory reaches the sliding surface, it stays on it and slides along it toward the origin. The system trajectory sliding along the sliding surface toward the origin is the sliding mode. The insensitivity of the controlled system to uncertainties exists in the sliding mode, but not during the reaching phase. Thus, the system dynamic in the reaching phase continues to be influenced by uncertainties [20-22].

Without loss of generality, consider the design of a sliding mode controller for the following second order system: $\ddot{x} + a_1 \dot{x} + a_2 x = b \cdot u$, where $u(t)$ is the input to the system, and b>0 is assumed. A possible choice for the structure of a sliding mode controller is [20-22]

$$u = u_{eq} + k \cdot \text{sgn}\left(s\right) \tag{24}$$

where u_{eq} is called the equivalent control, which dictates the motion of the state trajectory along the sliding surface

[20, 21]; k is a constant, representing the maximum controller output required to overcome parameter uncertainties and disturbances; and s is called the switching function because the control action switches its sign on the two sides of the switching surface $s=0$. A second-order system *s* is defined as [21, 22]:

$$s=\dot{e}+\lambda\cdot e \tag{25}$$

where $e=x_d-x$ and x_d are the desired states; λ is a constant; and *sgn(s)* is the signum function:

$$\operatorname{sgn}(s)=\begin{cases}-1 & s<0\\ 1 & s>0\end{cases} \tag{26}$$

To ensure that the system trajectories move toward and stay on the sliding surface $s=0$ independent of the initial condition, the following sliding mode condition must be fulfilled [20, 21, 26]:

$$s\dot{s}\le-\eta\cdot|s|\Rightarrow s\dot{s}\le-\eta\cdot\operatorname{sgn}(s)s\Rightarrow\dot{s}\cdot\operatorname{sgn}(s)\le-\eta \tag{27}$$

where η is a positive constant that ensures a finite time convergence to $s=0$.

In practice, using a sign function often causes chattering. One solution is to introduce a boundary layer around the switching surface [21, 25, 26]:

$$u=u_s+u_{eq} \tag{28}$$

where

$$u_s=k\cdot sat\left(s/\xi\right) \tag{29}$$

and where the constant factor ξ defines the thickness of the boundary layer, and $sat(\cdot)$ is a saturation function defined as

$$sat\left(s/\xi\right)=\begin{cases}\operatorname{sgn}\left(\dfrac{s}{\xi}\right) & \left|\dfrac{s}{\xi}\right|\ge 1\\ \dfrac{s}{\xi} & \left|\dfrac{s}{\xi}\right|<1\end{cases} \tag{30}$$

The characteristic of u_s versus s is shown in Fig. 4.

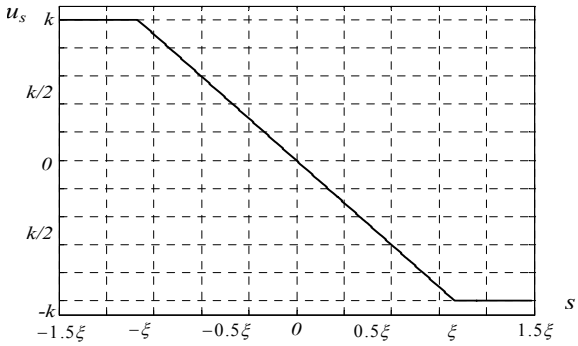

Fig. 4. Discontinuous control action of the SMC control law (u_s)

3.2 Design of speed and current controllers using SMC

The LIM has a significant nonlinear behavior, such as the coupling between the motor speed and the electrical quantities; the model parameters such as the mover mass and the friction coefficient may also not be exactly known. At the same time, the load thrust is always unknown. Other factors may also influence the LIM system. For example, the LIM is often influenced by parameter uncertainties because of the end effects, unmodelled dynamics, and external disturbances. The need for controllers with high performance and guaranteed robustness has increased during the last decade, especially with the requirement of high precision in real applications.

This section describes the design procedure of the robust nonlinear control via the SMC for LIM control, considering the end effects. The objective of this controller is to obtain the LIM control laws so as to achieve high-quality speed tracking performance. The design of the proposed sliding mode controller for an LIM mover speed control involves the following steps:

3.2.1 Design of sliding mode speed controller

To control the speed of the LIM, the sliding surface is defined as follows:

$$s(v_r)=v_r^*-v_r \tag{31}$$

Differentiating $s(v_r)$ with respect to time gives

$$\dot{s}(v_r)=\dot{v}_r^*-\dot{v}_r \tag{32}$$

Considering the motion equation of the LIM defined in Eq. (14), the time derivative of sliding surface can be written as

$$\dot{s}(v_r)=\dot{v}_r^*-\left(\frac{3}{2}\frac{PL_m(Q)\pi\cdot\phi_{dr}^*}{M\cdot h\cdot L_r(Q)}i_{qs}-\frac{D}{M}v_r-\frac{F_L}{M}\right) \tag{33}$$

We take

$$i_{qs}=i_{qs}^{equ}+i_{qs}^{n} \tag{34}$$

During the sliding mode and at steady-state conditions, $s(v_r)=0$, $\dot{s}(v_r)=0$, and $i_{qs}^{n}=0$; the equivalent control action can be defined as follows:

$$i_{qs}^{equ}=\frac{2}{3}\frac{hML_r(Q)}{\pi PL_m(Q)\phi_{dr}^{*}}\left(\dot{v}_r^{*}+\frac{D}{M}v_r+\frac{F_L}{M}\right) \tag{35}$$

During the convergence mode, the condition $s(v_r)\cdot\dot{s}(v_r)<0$ must be verified, thereby guaranteeing motion of the state trajectory to the manifold. Substituting (35) into the time derivative of the sliding surface $\dot{s}(v_r)$ yields

$$\dot{s}(v_r)=-\frac{3}{2}\frac{P\pi L_m(Q)\phi_{dr}^{*}}{hML_r(Q)}i_{qs}^{n} \tag{36}$$

The discontinuous control action can be given as

$$i_{qs}^{n}=k_{iqs}\cdot sat\left(s(v_r)/\xi_v\right) \tag{37}$$

To verify the system stability condition ($s(v_r)\cdot\dot{s}(v_r)<0$), choosing a strictly positive gain k_{iqs} is sufficient.

3.2.2 Design of sliding mode current controllers

The current loops are often the internal regulated loop in a field-oriented controlled LIM. The global performance of the drive is strongly dependent on the performance of current control. Therefore, precise and fast current control is essential to achieve high static and dynamic performance for the FOC of LIMs. If the secondary currents are not adjusted precisely and do not have fast dynamics to the reference values, cross-coupling will occur between the motor thrust and the primary flux, thereby degrading the performance of the FOC [16, 22].

The proposed control design uses two sliding mode controllers to regulate the d-axis and q-axis secondary currents. The design of the controllers consists of two steps.

First, the sliding surfaces $s=\begin{bmatrix}s_1 & s_2\end{bmatrix}=0$ are defined as follows:

$$s_1=i_{ds}^{*}-i_{ds} \tag{38}$$

$$s_2=i_{qs}^{*}-i_{qs} \tag{39}$$

where i_{ds}^{*} and i_{qs}^{*} are the reference values of the d-axis and *q*-axis secondary currents, respectively. If the system stays stationary on the surface, $s_1=s_2=0$ is obtained. Substituting (38) and (39) into $s_1=0$ and $s_2=0$, respectively, yields

$$\begin{aligned} i_{ds}&=i_{ds}^{*}\\ i_{qs}&=i_{qs}^{*}\end{aligned} \tag{40}$$

Second, a voltage-control law that forces the system to move towards the sliding surface in a finite time is designed.

Differentiating s_1 and s_2 with respect to time gives

$$\begin{aligned}\dot{s}_1&=\dot{i}_{ds}^{*}-\dot{i}_{ds}\\ \dot{s}_2&=\dot{i}_{qs}^{*}-\dot{i}_{qs}\end{aligned} \tag{41}$$

Taking into account the equations of the LIM defined in (6) and (7), the time derivative of the sliding surface can be written as follows:

$$\begin{aligned}\dot{s}_1=\dot{i}_{ds}^{*}-\frac{1}{L_\sigma(Q)}\Bigg(&-\left(R_s+\left(\frac{L_m(Q)}{L_r(Q)}\right)^2R_r\right)\cdot i_{ds}\\&+L_\sigma(Q)\cdot\frac{\pi}{h}\cdot v_e\cdot i_{qs}+\frac{L_m(Q)\cdot R_r}{L_r(Q)^2}\cdot\phi_{dr}+V_{ds}\Bigg)\end{aligned} \tag{42}$$

$$\begin{aligned}\dot{s}_2=\dot{i}_{qs}^{*}-\frac{1}{L_\sigma(Q)}\Bigg(&-L_\sigma(Q)\cdot\frac{\pi}{h}\cdot v_e\cdot i_{ds}\\&-\left(R_s+\left(\frac{L_m(Q)}{L_r(Q)}\right)^2\cdot R_r\right)\cdot i_{qs}\\&-\frac{P\cdot L_m(Q)\cdot\pi}{L_r(Q)\cdot h}\phi_{dr}\cdot v_r+V_{qs}\Bigg)\end{aligned} \tag{43}$$

We take

$$\begin{aligned}v_{qs}&=v_{qs}^{equ}+v_{qs}^{n}\\ v_{ds}&=v_{ds}^{equ}+v_{ds}^{n}\end{aligned} \tag{44}$$

During the sliding mode and at steady-state conditions, $s_1=\dot{s}_1=0$, $s_2=\dot{s}_2=0$, $v_{ds}^{n}=0$, and $v_{qs}^{n}=0$, the equivalent control actions can be defined as follows:

$$\begin{aligned}V_{ds}^{equ}=L_\sigma(Q)\Bigg(&\dot{i}_{ds}^{*}+\frac{1}{L_\sigma(Q)}\left(R_S+R_r\cdot\left(\frac{L_m(Q)}{L_r(Q)}\right)^2\right).i_{ds}\\&-\frac{\pi}{h}v_e.i_{qs}-\frac{L_m(Q).R_r}{L_\sigma(Q)L_r^2(Q)}\phi_r^{*}\Bigg)\end{aligned} \tag{45}$$

$$\begin{aligned}V_{qs}^{equ}=L_\sigma(Q)\Bigg(&i_{qs}^{*}+\frac{\pi}{h}v_e.i_{ds}+\frac{1}{L_\sigma(Q)}\left(R_s+R_r\left(\frac{L_m(Q)}{L_r(Q)}\right)^2\right).i_{qs}\\&+\frac{L_m(Q)}{L_\sigma(Q)L_r(Q)}\phi_r^{*}\frac{\pi}{h}v_r\Bigg)\end{aligned} \tag{46}$$

During the convergence mode, the conditions $s_1\cdot\dot{s}_1<0$ and $s_2\cdot\dot{s}_2<0$ must be verified to guarantee the motion of

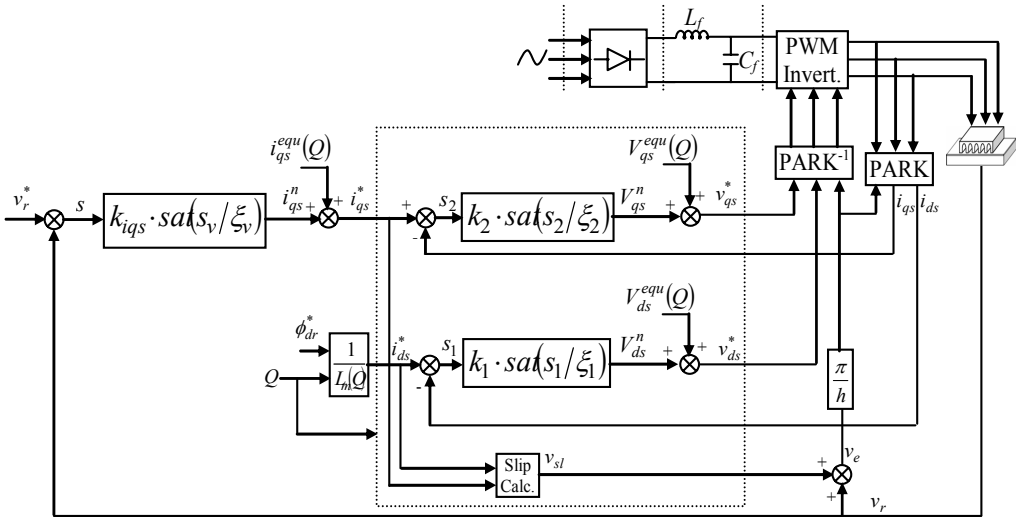

Fig. 5. Block diagram of sliding mode speed and currents control of LIM with end effects compensation

the state trajectory to the manifold. Substituting (45) and (46) into the time derivatives of the sliding surfaces $\dot{s}_1$ and $\dot{s}_2$, respectively, yields

$$\begin{aligned} \dot{s}_1 &= -\frac{1}{L_\sigma(Q)} v_{ds}^n \\ \dot{s}_2 &= -\frac{1}{L_\sigma(Q)} v_{qs}^n \end{aligned} \tag{47}$$

The discontinuous control actions can be given as

$$\begin{aligned} v_{ds}^n &= k_1 \cdot sat\left(s_1/\xi_1\right) \\ v_{qs}^n &= k_2 \cdot sat\left(s_2/\xi_2\right) \end{aligned} \tag{48}$$

To verify the system stability condition ($s_1 \cdot \dot{s}_1 < 0$, $s_2 \cdot \dot{s}_2 < 0$), choosing strictly positive and sufficiently large gains k_1 and k_2 are sufficient.

4. Simulation results

Simulations were carried out in MATLAB/SIMULINK to demonstrate the effectiveness of the proposed control scheme for speed control of the LIM. The block diagram of the proposed control system is shown in Fig. 5. The proposed control system mainly consists of a linear induction motor, a ramp comparison current-controlled pulse width modulated (PWM) inverter, a slip velocity estimator, an inverse park, IFOC bloc based on sliding mode current controller, and a speed feedback control loop that contains a sliding mode controller.

First, the simulated results of the proposed sliding mode control system for a rectangular shape-thrust command input and step reference for speed control are presented. The parameter used in the simulation were chosen as $k_{iqs} = 25$, $k_2 = k_3 = 40$, $\xi_{vr} = 0.5$, and $\xi_1 = \xi_2 = 0.1$. These parameters were chosen to achieve the best transient control performance in the simulation considering the requirement of stability and possible operating conditions.

Fig. 6 shows the magnetizing inductance $L_m\left(1-f\left(Q\right)\right)$ and thrust coefficient $L_m\left(1-f\left(Q\right)\right)/\left(L_r - Lm\cdot f\left(Q\right)\right)$ against speed. A noticeable reduction of the magnetizing inductance was observed with increase of v_r, whereas the thrust coefficient remained nearly invariant. The simulated results of the SMC system with and without consideration on end effects for a rectangular shape-thrust are shown in Fig. 7. The thrust is depicted in Fig. 7(a), and the direct

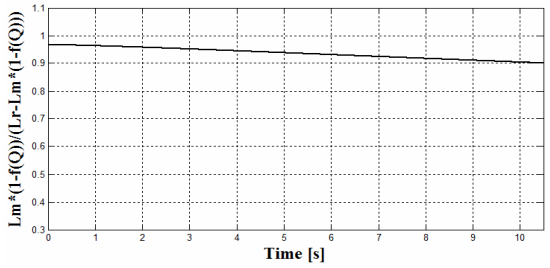

(a)

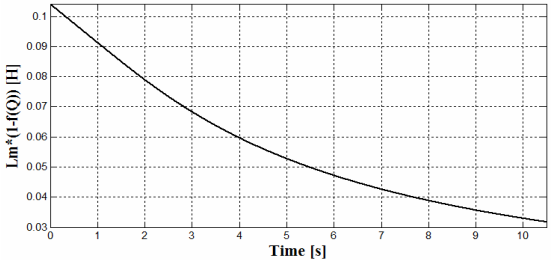

(b)

Fig. 6. Magnetizing inductance and thrust coefficient against speed: (a) Magnetizing inductance; (b) Thrust coefficient

secondary current i_{ds} is depicted in Fig. 7(d). Figs. 7(b) and 7(c) show the direct and quadratic secondary fluxes ϕ_{dr} and ϕ_{qr}, respectively.

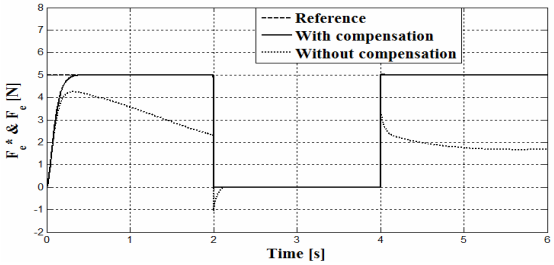

(a)

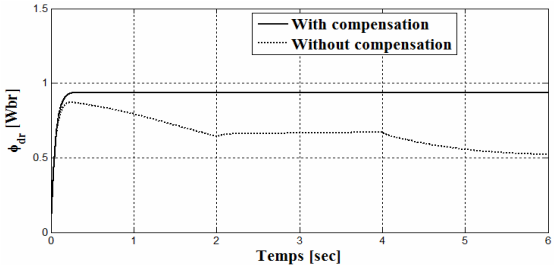

(b)

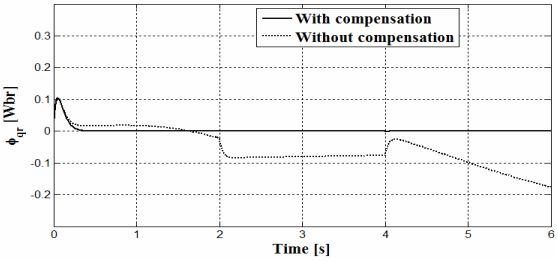

(c)

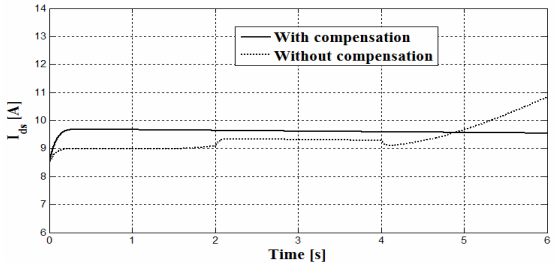

(d)

Fig. 7. Simulated results of the decoupling obtained by SMC with and without end effects compensation

With the conventional SMC, the flux level decreases as the speed increases. The thrust cannot track the rectangular shaped-thrust reference; thus, poor decoupled property is obtained. The fluxes cannot precisely track the desired fluxes because of the variation in the parameters (L_m, L_s, and L_r). In contrast, with the proposed scheme, the flux level is kept constant and no discrepancy is observed between the thrust command and the produced thrust. The same remarks are observed for the d-axis current. However, to keep the flux constant, i_{ds} needs to be compensated as motor speed increases or decreases.

To further demonstrate the control performance of the proposed control scheme for speed control, the simulated results of the conventional and the proposed sliding mode control systems because of a step command are given in Figs. 8(a)-8(d). From the simulated results shown in Fig. 8, the proposed SMC scheme can achieve favorable tracking performance even in relation to load force disturbance variation. In Figs. 8(a)-8(d), the speed response of the proposed SMC is observed to present better tracking

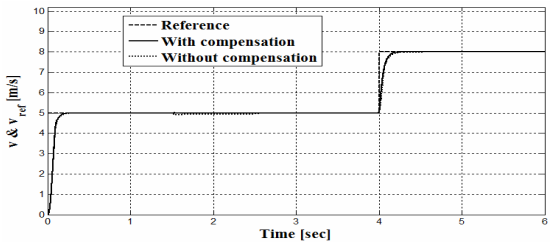

(a)

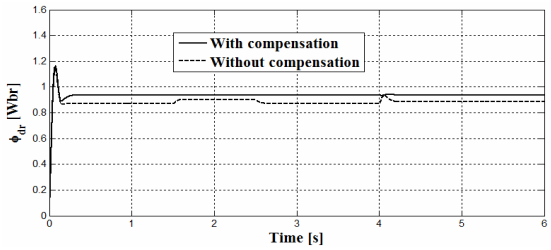

(b)

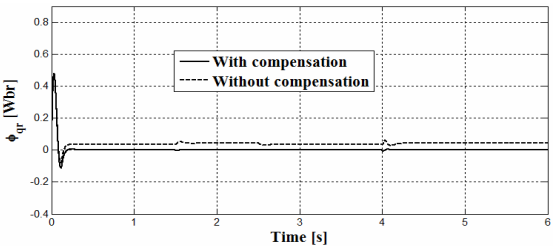

(c)

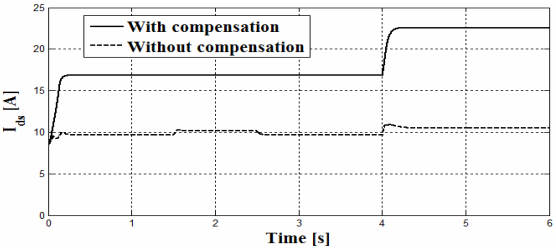

(d)

Fig. 8. Simulated results of the speed control using SMC with and without end effects compensation

characteristics and more robustness compared with that of the conventional sliding mode controller (without end effects compensation). In addition, the influence of external disturbance on the speed response of the mover is much reduced; better decoupled properties are obtained, and the fluxes are able to track the desired fluxes precisely. With the conventional sliding mode controller, secondary flux is linearly proportional to the primary d-axis current in the steady state (i.e., $\phi_{dr}^{*} = L_m i_{ds}^{*}$). However, with the complete model of the LIM, the coefficient depends strongly on the velocity (i.e., such that $\phi_{dr} = L_m \left(1 - f\left(Q\right)\right) i_{ds}$ in the steady state). In this case, the flux ϕ_{dr} for a given i_{ds} decreases as the LIM velocity v_r increases, and increases as the LIM velocity decreases. Hence, to keep the flux constant, i_{ds} must be compensated as motor speed increases or decreases. Now, the proposed control scheme and the conventional sliding mode controller are simulated and compared under the same drive conditions. The simulated results because of step reference signal are shown in Fig. 9. The proposed control system presents favorable tracking characteristics under load force application (minimal steady state errors, minimal rise time, and best disturbance rejection for the proposed controller).

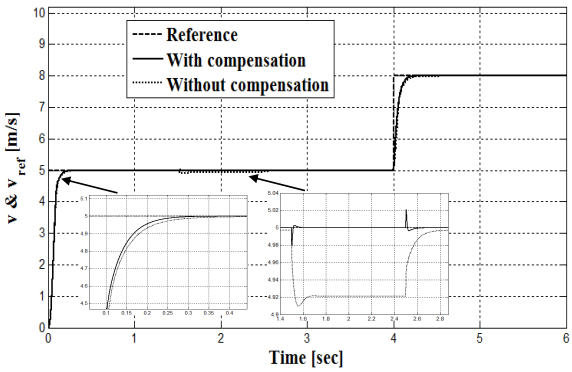

Fig. 9. Speed response using sliding mode control (Zoomed responses)

To further demonstrate the control performance of the proposed control scheme, the compensated and the conventional sliding control systems are simulated with secondary resistance and magnetizing inductance variations. In this simulation, the proposed system is simulated with an increasing value of the nominal secondary resistance R_r and magnetizing inductance of the LIM (R_r=1.5xR_{rN}, L_m=1.5xL_{mN}). The tracking responses of the conventional SMC system shown in Fig. 10(a)-10(d) and Fig. 11(a)-11(d) are more sensitive to secondary resistance, magnetizing inductance variations, and time-varying external force disturbance. Furthermore, non-ideal decoupled characteristic are induced under the occurrence of the external load disturbance. Conversely, in Figs. 10(a)-10(d) and 11(a)-11(d), the speed response of the proposed sliding mode controller presents better tracking characteristics, has minor sensitivity to the secondary resistance and magnetizing inductance variation, and is more robust than that of the conventional sliding mode controller. Therefore, the robust control performance of the proposed sliding mode controller both in the speed tracking and the load regulation are obvious. However, the proposed scheme is observed to need an adaptive control law or an estimation of the end effect and magnetizing inductance. Fig. 12 shows the $f(Q)$ function against time simulation. Clearly, the $f(Q)$ function level increases as the speed v_r increases.

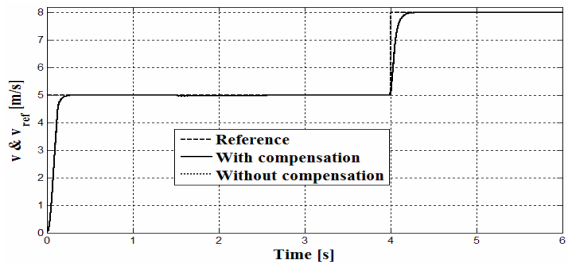

(a)

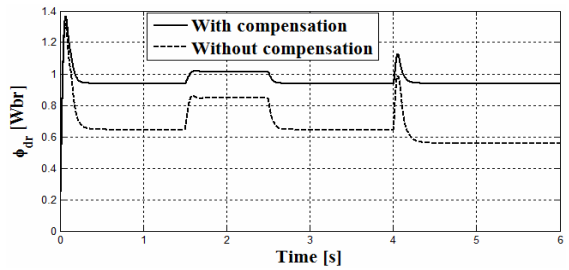

(b)

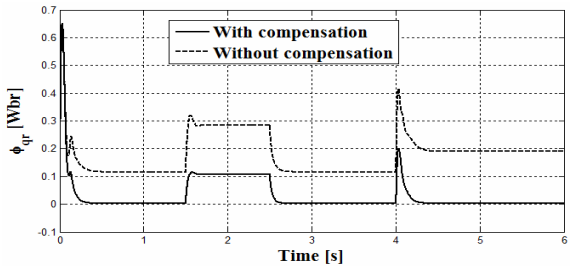

(c)

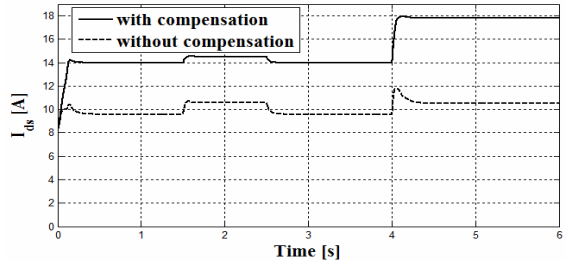

(d)

Fig. 10. Simulated results of the proposed and conventional sliding mode control for LIM speed tracking with secondary resistance value variation

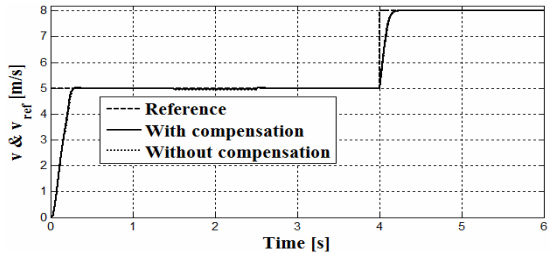

(a)

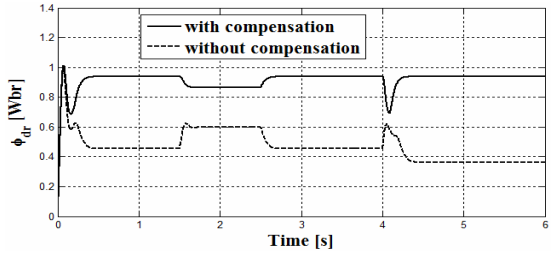

(b)

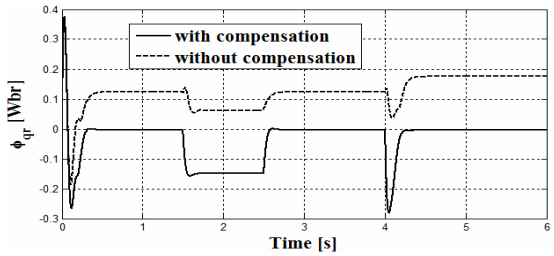

(c)

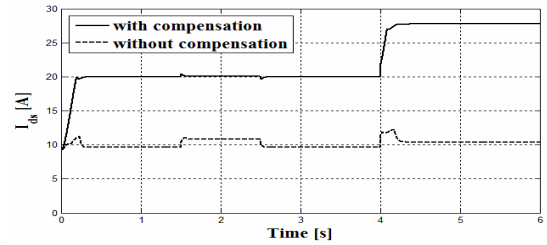

(d)

Fig. 11. Simulated results of the proposed and conventional SMC for LIM speed tracking with magnetizing inductance value variation

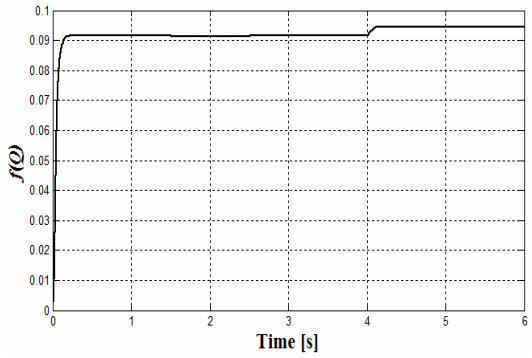

Fig. 12. $f(Q)$ function

5. Conclusion

The present paper demonstrates the application of a nonlinear SMC system for the speed control of an LIM, considering end effects. First, an IFOC of LIM is designed, considering the end effects. Moreover, a SMC design technique is investigated to achieve a thrust-, flux-, and speed-tracking objective under disturbance of load thrust force. The control dynamics of the proposed hierarchical structure were investigated through numerical simulation. The proposed sliding mode controller with end effects compensation presented satisfactory performances and provided desirable decoupling between flux and thrust. However, the proposed scheme needs an adaptive control law or an estimation of the end effect and magnetizing inductance.

Appendix

Table 1. LIM Parameters

ϕ_{2S} [Wb]	0.9378	L_s [H]	0.1078
R_s [Ω]	0.34	f_n [Hz]	50
R_r [Ω]	0.195	M [kg]	5.47
L_r [H]	0.1078	D [Nm.s/rd]	26.36
L_m [H]	0.1042	P	2

List of abbreviations and acronyms

i_{ds}, i_{qs} : Direct and quadrature secondary currents
k_p, k_i : Proportional and integral actions of PI controllers
L_s, L_r, L_m : Primary, secondary, and magnetizing inductances
L_{lr}, L_{ls} : Primary and secondary leakage inductances
P : Number of pairs of poles
R_s , R_r : Primary and secondary resistances
D : Viscous friction and iron-loss coefficient
M : The total mass of the moving element
v_{ds} , v_{qs} : Direct and quadrature primary voltages
ϕ_{dr} , ϕ_{qr} : Direct and quadrature secondary fluxes
i_{qs}^* , i_{ds}^* : q-axis and d-axis primary currents command
τ_r : Secondary time constant (L_r / R_r)
v_e : Synchronous velocity
v_r : Mover linear velocity
v_{sl} : Slip velocity
Q : Dimensionless factor
l : Primary length
h : Pole pitch
F_e : Thrust force
K_f : Constant force
F_L : Load force
LIM : Linear Induction Motor
RIM : Rotary Induction Motor
IFOC : Indirect Field-Oriented Control
SMC : Sliding Mode Control
DC : Direct Current

IM : Induction Motor
AC : Alternative Current

References

[1] P. -K. Huang, Recurrent fuzzy neural network controlled linear induction motor drive based on genetic algorithm, Master Thesis, Chung Yuan Christian University, 2002.

[2] C. -Y. Hung, Adaptive control for rotary induction motor and linear induction motors, Master Thesis, Chung Yuan Christian University 2001.

[3] R. J. Kaye and E. Masada, Comparison of Linear Synchronous and Induction Motors, Urban Maglev Technology Development Program Colorado Maglev Project, Internal Rapport, 2004.

[4] S. P. Bhamidi, Design of a Single Sided Linear Induction Motor (Slim) Using A User Interactive Computer Program, Master Thesis, Missouri-Colombia University, 2005.

[5] R. -J. Wai and W. -K. Liu, "Nonlinear Decoupled Control For Linear Induction Motor Servo-Drive Using The Sliding-Mode Technique", IEE Proc. Control Theory Application, Vol. 148, No. 3, 2001, pp. 217-231.

[6] E. F. da Silva, E. B. dos Santos, P. C. M. Machado, M. A. A. de Oliveira, "Dynamic Model for Linear Induction Motors", IEEE Proc. of ICIT 2003, Maribor (Slovenia), 2003, pp. 478-482.

[7] J. -H. Sung and K. Nam, "A New Approach to Vector Control for a Linear Induction Motor Considering End Effects", IEEE IAS annual meeting, 3-7 Oct, in Phoenix, Arizona, 1999, pp. 2284-2289.

[8] G. Kang and K. Nam, "Field-oriented control scheme for linear induction motor with the end effect", IEE Proc. Electr. Power Appl., Vol. 152, No. 6, November 2005, pp. 1565-1572.

[9] J. Liu, F. Lin, Z. Yang, T. Q. Zheng, "Field-Oriented Control of Linear Induction Motor Considering Attraction Force & End-Effects", IEEE Proc. Of IPEMC 2006.

[10] S. Vaez-Zadeh, M. R. Satvati, "Vector Control of Linear Induction Motors with End Effect Compensation", The Eight International Conference on Electrical Machines and Systems (ICEMS), 2005, pp. 635-638.

[11] Z. Zhang, Eastham, T. R. and G. E., Dawson, "Peak thrust operation of linear induction machines from parameter identification". Proc. IEEE, IASC, 1995, pp. 375-379

[12] B. Kwon, K. Woo, S. Kim. "Finite Element Analysis of Direct Thrust-controlled Linear induction motor", pp, 1306-1309, IEEE Trans. on Magnetics, Vol. 35, N° 3, 1999.

[13] R. C. Creppe, "Dynamic Behavior of a linear induction Motor", Proc. Of Medifterranean Electrotechnical Conference, Vol. 2, 1998.

[14] N. Fujii, T. Kayasuga and T. Hoshi, "Simple End Effect Compensator for Linear Induction Motor", IEEE Trans. On Mag., Vol. 38, N° 5, September 2002, pp. 3270-272.

[15] B. K. Bose, Modern Power Electronics and AC Drives, Printice Hall PTR, USA, 2002, ISBN 0-13-016743-6.

[16] J. P. Caron and J. P. Hautier (1995), Modelling and Control of Induction Machine, Technip Edition, France (text in french).

[17] F. -J. Lin, D. -H. Wang and P. -K. Huang, "FPGA-Based Fuzzy Sliding-Mode Control For A Linear Induction Motor Drive", IEE Proc. Electr. Power Appl., Vol. 152, No. 5, 2005, pp. 1137-1148.

[18] F. -J. Lin, P. -H. Shen and S. -P. Hsu, "Adaptive backstepping sliding mode control for linear induction motor", IEE Proc. Electr. Power Appl., Vol. 149, No. 3, pp. 184-194, May 2002.

[19] F. -J. Lin, R. -J. Wai, W. -D. Chou, and S. -P. Hsu, "Adaptive Backstepping Control Using Recurrent Neural Network for Linear Induction Motor Drive", IEEE Trans. on Ind. Elect., Vol. 49, No 1, 2002, pp. 134-146.

[20] V. I. Utkin, "Sliding Mode Control Design Principles and Applications to Electric Drives", IEEE Trans. Ind. Electr., Vol. 40. N° 01, 1993, pp. 23-36.

[21] J. J., Slotine, Applied Nonlinear Control, Prentice-Hall. Inc., 1991, ISBN 0-13-040890-5.

[22] R. -J. Wai, "Adaptive Sliding-Mode Control for Induction Servomotor Drives", IEE Proc. Elect. Power Appl., 2000, Vol. 147, pp. 553-562.

[23] J. Soltani, and M. A. Abbasian, "Robust Nonlinear Control of Linear Induction Motor Taking Into Account the Primary End-Effects", IEEE Proc. Of IPEMC, 2006, pp. 1-6.

[24] C. -M. Lin and C. -F. Hsu, "Adaptive Fuzzy Sliding-Mode Control for Induction Servomotor Systems", IEEE Transactions on Energy Conversion, vol. 19, n°2, June 2004, pp. 362-368

[25] R. -J. Wai, C. -M. Lin and C. -F. Hsu, "Adaptive Fuzzy Sliding-Mode Control for Electrical Servo Drives", Fuzzy Sets and Systems 143, 2004, 295-310.

[26] S. G., Tzafestas and G. G., Rigatos, "Design and Stability Analysis of a New Sliding-Mode Fuzzy Logic Controller of Reduced Complexity", Machine Intelligence & Robotic Control, Vol. 1, No. 1, 1999, pp. 27-41.

Boucheta Abdelkrim received his B.S. and M.S. degrees in Electrical Engineering from the Electrical Engineering Institute of the University Center of Bechar in 2001 and 2006, respectively. He then received his Ph.D degree in Electrical Engineering from the University of Djilali Liabes Sidi-Belabbes (Algeria) in 2010. He is currently a Professor of Electrical Engineering at the University of Bechar, Bechar, Algeria. His areas of interest include modern and adaptive control and their application in linear electric drives control.

Bousserhane Ismail Khalil received his B.S. degree in Electrical Engineering from the Electrical Engineering Institute of the University Center of Bechar in 2000. He then received his MS and Ph.D degrees in Electrical Engineering from the University of Sciences and Technology of Oran (Algeria) in 2003 and 2008, respectively. He is currently a Professor of Electrical Engineering at the University of Bechar, Bechar, Algeria. His areas of interest include modern control techniques and their application in electric drives control.

Hazzab Abdeldjebar received his State Engineer, M.S., and Ph.D degrees in Electrical Engineering from the Electrical Engineering Institute of The University of Sciences and Technology of Oran (USTO), Algeria in 1995, 1999, and 2006, respectively. He is currently a Professor of Electrical Engineering at the University of Bechar, Bechar (Algeria), where he has been the Director of the Research Laboratory of the Command, Analyses, and Optimization of Electro-Energetic Systems since 2009. His research interests include power quality, modeling, modern controller and observer design for nonlinear systems, control of power electronics, multidrive systems and electrical vehicle, and adaptive control and no-linear systems diagnostic.

Pierre Sicard received his Bachelor in Technology of Electricity from the Ecole de Technologie Supérieure, Montréal QC, Canada in 1985, his MSc in Industrial Electronics from the University of Québec in Trois-Rivières, Trois-Rivières QC, Canada in 1990, and his PhD in Electrical Engineering from Rensselaer Polytechnic Institute, Troy, New York, USA in 1993. In 1992, he joined the University of Québec in Trois-Rivières as a Professor in Electrical and Computer Engineering, where he has been the Director of the Research Group in Industrial Electronics since 2004. His research interests include power quality, modeling, controller and observer design for nonlinear systems, control of power electronics and multidrive systems, passivity-based control, adaptive control, and neural networks.

Mohammed Karim Fellah received the Eng. degree in Electrical Engineering from the University of Sciences and Technology, Oran, Algeria in 1986, and his Ph.D degree from the National Polytechnic Institute of Lorraine (Nancy, France) in 1991. Since 1992, he has been a professor at Djillali Liabès University of Sidi-bel-Abbès (Algeria). He was the Director of the Intelligent Control and Electrical Power Systems Laboratory at this University from 2000 to 2010. Today, he remains a member of this laboratory. His current research interest includes power electronics, HVDC links, and drives.